Modelling structural determinants of ventilation heterogeneity: a perturbative approach.

Carl A. Whitfield*[1,2], Alex Horsley[1], and Oliver E. Jensen[2]

[1]Division of Infection, Immunity and Respiratory Medicine, University of Manchester, Southmoor Road, Manchester, UK, M23 9LT

[2]School of Mathematics, University of Manchester, Oxford Road, Manchester, M13 9PL

Abstract

We have developed a computational model of gas mixing and ventilation in the human lung represented as a bifurcating network. We have simulated multiple-breath washout (MBW), a clinical test for measuring ventilation heterogeneity in patients with obstructive lung conditions. By applying airway constrictions inter-regionally, we have predicted the response of MBW indices to obstructions and found that they detect a narrow range of severe constrictions that reduce airway radius to between 10% -30% of healthy values. These results help to explain the success of the MBW test to distinguish obstructive lung conditions from healthy controls. Further, we have used a perturbative approach to account for intra-regional airway heterogeneity that avoids modelling each airway individually. We have found, for random airway heterogeneity, that the variance in MBW indices is greater when large-magnitude constrictions are already present, and that the indices become more sensitive to structural heterogeneity when already elevated. This method is a computationally efficient way to probe the lung's sensitivity to structural changes, and to quantify uncertainty in predictions due to random variations in lung mechanical and structural properties.

Author summary

The multiple-breath washout (MBW) test is a clinical test of lung function that measures the efficiency of gas transport and mixing within the lung, and which has proven very sensitive in detecting early disease in cystic fibrosis (CF). In this paper we have developed a computational model of lung function to simulate air movement and gas transport in the lungs and generate MBW outcomes. We have used this to show why MBW is so sensitive to airway blockages similar to those encountered in CF.

Importantly, the model incorporates a new and computationally-efficient method that also allows us to account for uncertainty and randomness in lung structure and mechanical properties. This has been used to show how variability of MBW outcomes increases in disease states. The model provides a framework for modelling clinical data, where accounting for uncertainties in inputs is crucial in making clinically meaningful predictions.

*carl.whitfield@physics.org

Introduction

The relationship between structure and function in the human lung is an important research area in physiology and medicine. Weibel's casts of human lungs demonstrated that the bronchial tree can be treated as consisting of two functional regions [1]. First, the relatively rigid conducting part of the tree consists of dichotomously branching tubes that, on average, approximately follow the self-similar branching pattern given by Murray's Law [2] allowing efficient transport of gas to the distal part of the lung. Second, the respiratory part of the lung (the acini) continues the dichotomously branching pattern but the tube lengths and diameters deviate from Murray's law and airways terminate in alveolar sacs, where gas transfer with blood takes place [3]. The result is that flow velocity drops off very quickly in the acini and diffusion transports gas through the alveoli.

Ventilation heterogeneity (VH) arises in various obstructive lung diseases, such as cystic fibrosis (CF) and asthma, where inhaled gas is unevenly distributed in the lung, leading to poorer gas mixing efficiency [4, 5]. The severity of these conditions, in particular CF, is often quantified clinically using Multiple Breath Washout (MBW) tests [6]. MBW uses an inert tracer gas to quantify how effectively fresh air is turned over in the lung by measuring the tracer gas concentration and flow rate at the mouth. These data are used to compute clinically tested indices such as the lung clearance index (LCI) and phase-III slopes [7], which are indicators of VH.

Modelling the results of MBW tests accurately is challenging. First, modelling gas flows in a heterogeneous lung structure is a computationally expensive task. According to cast estimates there are on the order of $10^4 - 10^5$ branches in the conducting zone [8, 9], and on the order of 10^7 including the acinar ducts. There have been numerous approaches to resolve this problem, such as using a symmetric description with an effective diffusion coefficient to account for heterogeneous ventilation [10], compartmental models with asynchronous or asymmetric ventilation [11, 12, 13], modelling a single heterogeneous acinus [14, 15], and replacing the acini with well mixed units or symmetric models reducing the computation to $\sim 10^4$ branches [16, 17, 18, 19, 20]. Models have considered both heterogeneity in healthy lungs (such that average diameters and lengths converge to the healthy lung data) and pathological heterogeneity (where branches are constricted on average). Secondly, the majority of model parameters are difficult to measure experimentally, and are variable between subjects, which increases the uncertainty in predictions.

In this paper, we outline a perturbative approach to account for weak heterogeneity and the resulting uncertainty in ventilation within the lung. In this limit, gas transport can be estimated by a linear superposition of the solutions on trees with individual perturbations, greatly reducing computational expense. We simulate only the linearised response to perturbations and use these post-hoc to compute the response to different distributions of heterogeneity. The underlying physiological model we present assumes a linear elastic response of the alveoli, and Poiseuille flow throughout. However, the approach we present is generic and will be used in the future to quantify uncertainty and model the effects of heterogeneity in more complex constitutive models.

The perturbative approach can be used to describe lung structures with heterogeneity that is either deterministic (where the structural and mechanical properties are prescribed) or probabilistic (with properties described by multivariate distributions) within the same simulations. The probabilistic descriptions of lung structure means that we are able to directly estimate the variance of model outputs due to the parameter distributions and thus quantify uncertainty. We have applied this method to the particular case of MBW simulation.

In summary, the aim of this research was to model the complex mechanisms relating heterogeneity

and randomness in lung structure to MBW outcomes and their variability. To achieve this we had to develop an efficient method of accounting for weak structural heterogeneity that does not require simulating every airway and duct in the multi-scale lung structure individually.

Methods

Computational Lung Model

We have modelled the effects of inter-regional heterogeneity in the lung using a coupled network model of ventilation and gas transport in the airways and acinar ducts. To reduce model complexity, we have initially assumed that the airway tree can be approximated as completely symmetric within seven lung regions (see Figure 1); we refer to this as the mean-path model. Each region corresponds to a lobe or lobar compartment resembling the regions in Horsfield and Cumming's lung model A [9]. We define the Strahler order of an airway by the maximum number of generations distal to it including acinar duct generations (counting from zero). Details of the model and parameters used can be found in S1 File and are summarised in S1 Table.

Gas flow on the airway network is calculated using a coupled set of ordinary differential equations (ODEs) that account for airway resistance (assuming Poiseuille flow), linear viscoelasticity of the acinar units and a uniform applied pleural pressure (similar to [17, 21, 18]). These ODEs are solved directly using the Eigen [22] factorisation routine 'PartialPivLU' in C++, as outlined in detail in S1 File §1.2. The concentration of inert gas on the network is then calculated using a one-dimensional advection-diffusion equation (S1 File §1.3) that accounts for transport into the alveolar sacs (similar to [23, 14, 15]). Transport in the acinar airways is included in this description as the details of its structure are important to accurately model gas transport [24, 25, 26, 27]. Within each lobar region the transport equation is identical to the 'trumpet' representation introduced in [28] (S1 File §1.4), with effective diffusion in the conducting region given by Taylor-like dispersion described in [29]. In the acinar region, pure molecular diffusion is modelled but with a modified airway cross-section, as described in [15]. The transport partial differential equations (PDEs) are discretised using a finite volume method (detailed in S1 File §2), and solved iteratively using the Eigen [22] 'BiCGSTAB' routine.

This lung model was used to simulate a multiple-breath washout (MBW) test by modelling the transport of an inert gas concentration c on the lung network, where c was assumed to be initially uniformly distributed. We selected tidal volume, functional residual capacity (FRC), airway deadspace volumes and lung elasticity values that are representative of a healthy adult male (see S1 Table). The MBW test measures FRC from the total inert gas exhaled over the test [7], which we label as $V_{\mathrm{FRC}}^{\mathrm{approx}}$. The lung clearance index (LCI) value is taken to be the interpolated number of lung turnovers (exhaled volume in units of $V_{\mathrm{FRC}}^{\mathrm{approx}}$) required to reduce the concentration (measured at the mouth at end of exhalation) to 2.5% of its initial value. LCI is a widely tested clinical measure of ventilation heterogeneity [30, 31], with healthy values generally in the range 6–8 and larger values indicating increased heterogeneity. Interpolation is necessary to measure small changes in LCI that are below the resolution of clinical LCI measurements, which are restricted to the set of end-tidal volumes (see S1 File §3). Phase-III indices measure ventilation heterogeneity through the slope of the measured gas concentration versus exhaled volume during individual breaths, and their interpretation is informed by numerical modelling [32, 33, 34]. In this paper we focus on S_{cond}, the linear gradient of the normalised phase III slopes, measured according to the clinical guidelines for MBW in [7]. A

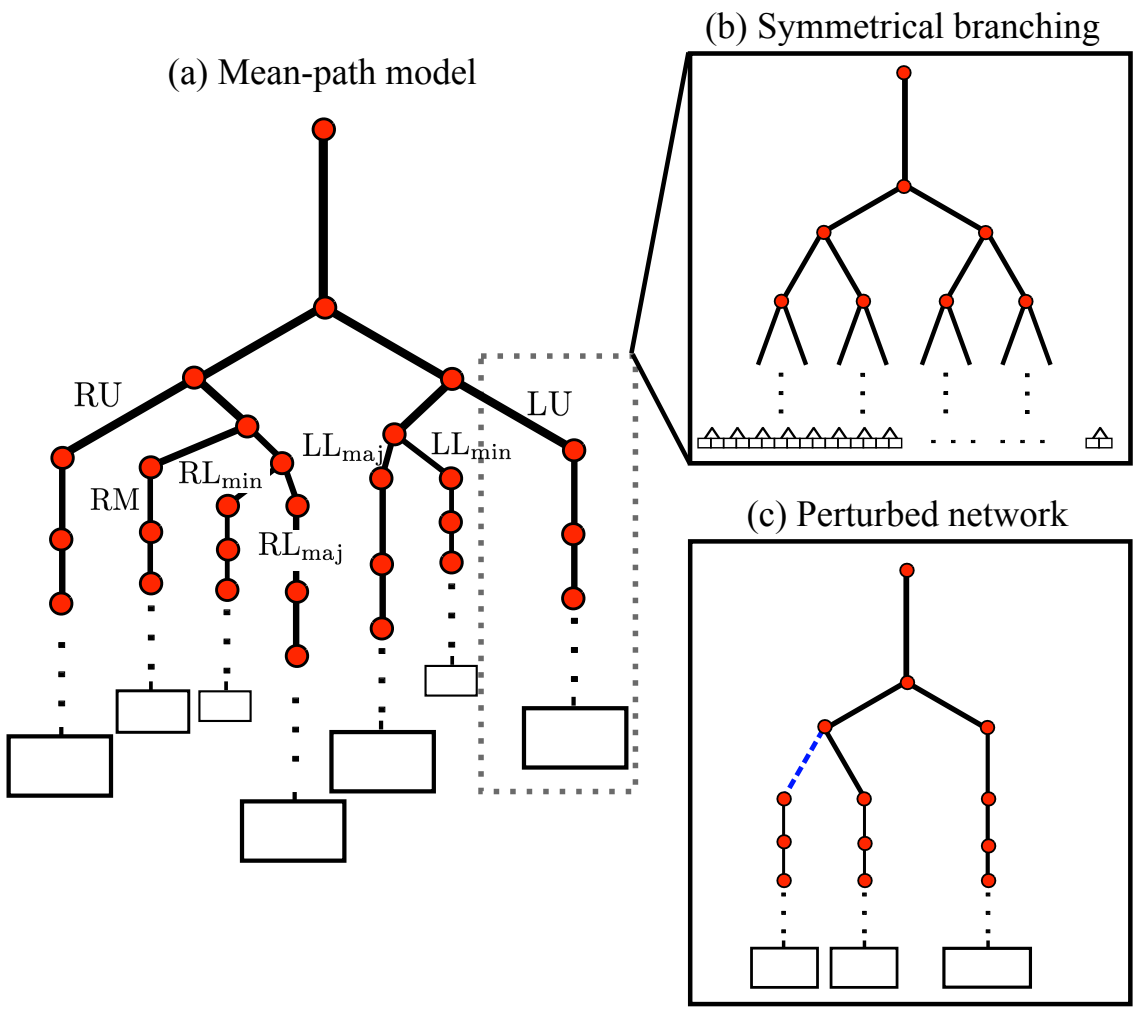

Figure 1: (a) Network diagram of the asymmetric model used to simulate MBW. Each mean-path (right-upper, RU; right-middle, RM; right-lower minor, RL_{min}, right-lower major, RL_{maj}; left-upper, LU; left-lower minor, LL_{min}; left-lower major, LL_{maj}) represents a symmetrically branching tree (shown in (b)) as a single path. Each black line represents an edge of the network, while each red dot is a vertex. The boxes indicate the parenchymal volume fed by each terminal airway or set of airways. (c) The mean-path is replaced with a perturbed network to calculate the linear response to a single airway deviating from the mean-path properties (shown for a perturbation in generation 2 of the mean-path, blue-dashed line).

more recent development in the field comes from hyperpolarised helium MRI imaging of the inert gas concentration in lungs [35]. Using this technique, fractional ventilation of lung acini is also quantified by calculating the dilution rate of the inert gas concentration between successive breaths at end-tidal volume [36]. Heterogeneity in fractional ventilation correlates strongly with increased LCI, but the MRI images can also identify changes not picked up by MBW indices, as well as provide important information about the spatial distribution of ventilation [6]. While the network model presented here cannot predict the spatial structure of FV distributions measured in MRI, it can predict distribution within each model region.

Perturbative method and application to structural heterogeneity

Building on this model, we have used perturbation theory to calculate the changes in gas concentration due to small variations of the properties of a single airway or acinus in a mean-path. This

involves calculating the linearised response of the simulation variables with respect to the perturbation magnitude, modelled by the dimensionless parameter $\epsilon \ll 1$. For example, if a given airway has cross-sectional area a in the baseline model, it becomes $a(1+\epsilon)$ in the perturbed case, and the response of all other simulation variables, such as gas concentration c, are computed to linear order in ϵ. For each perturbation considered, the number of separate paths that need to be simulated grows linearly with the airway generation number.

In "Intra-regional heterogeneity", we have used this method to model intra-regional heterogeneity in airway sizes, by assuming they are randomly distributed about their mean-path values, and that the variance of this distribution is small enough that we can apply perturbation theory as detailed in S1 File §1.5. In the simple case where the perturbations are modelled as variables in a multivariate Gaussian, the variance in model outputs can be computed as a sum of the covariance of inputs weighted by their respective linear sensitivities (see S1 File §3.) This gives a computationally efficient method to relate weak intra-regional heterogeneity to variance of model outputs that relies only on each constricted case being simulated once.

We have modelled uncorrelated, normally distributed perturbations to the area and length of the conducting airways. We have assumed that the coefficient of variation of these parameters, σ_a and σ_l, is independent of generation and path, (see S1 File §3.1 for a mathematical description of this distribution). We have also introduced structurally correlated uncertainty in geometry within each

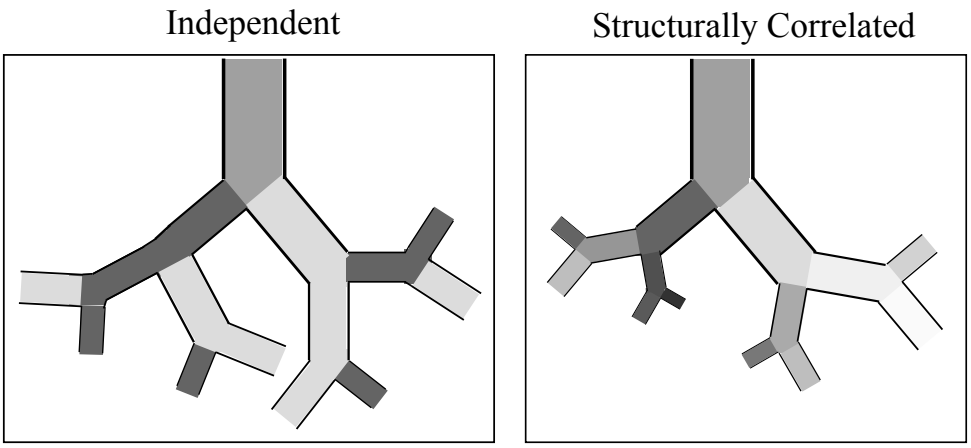

Figure 2: Sketch of randomly distributed airway sizes, shading (from dark to light) indicates airway size relative to generational average. In the independent case, variations in branch size are uncorrelated. In the correlated case larger than average airways are likely to beget airways that are also larger than average, resulting in an increased uncertainty in the size of the most distal airways. For simplicity, all airways in this sketch have fixed aspect ratio (the case $\rho_{al} = 1$). When $\rho_{al} = 0$, airway length and area are independent.

mean path. The assumption made here is that the deviation of each branch from the mean-path value is normally distributed around that of its parent branch (see Figure 2), again with coefficients of variation σ_a, σ_l. The area and length deviation of a branch is itself taken to be correlated with coefficient $-1 \leq \rho_{al} \leq 1$. In what follows we present the case $\sigma_a = 2\sigma_l$ (in the linear limit radius and length have the same coefficient of variance), for $\rho_{al} = 0$ (no area and length correlation) and $\rho_{al} = 1$ (fixed aspect ratio). A complete description of this case is given in S1 File §3.2. This case is similar to the random structure generated used for particle deposition calculations in [37], whereby airway sizes are generated according to the size of the parent airway.

Finally, we have used these results to compute the probability density of any acinus in the model

having a given FV value (averaged over the whole MBW test). In the limit of a large number of acini, the distribution of FV values in any given lung model realisation will tend towards this distribution (see S1 File §3 for further details).

Model validation

Validation studies to test the accuracy and precision of the numerical simulations can be found accompanying the source code at [45]. In these we have tested that the code is suitably converged for the choice of model time-step and space-step, and that inert gas volume is conserved. We also tested that the perturbative model converges exactly to the mean-path model in the limit of small perturbations.

Results

The healthy baseline model (Figure 1) assumed that all regions have the same airway sizes and mechanical properties. This resulted in a homogeneous distribution of gas, with the only asymmetry originating from the arrangement of the proximal airways supplying the lobar regions, and the number of generations within each region. In this case the simulations showed little regional difference in fractional ventilation and each lobe contributed proportionately to the washout. The baseline values of the MBW indices (using SF_6 as the tracer gas) were LCI = 5.16, $S_{\text{cond}} = 1.92 \times 10^{-4}\text{L}^{-1}$ and $V_{\text{FRC}}^{(\text{approx})} = 3.00\text{L}$ (to 3 s.f.). Using N_2 the LCI reduced slightly to 5.04, due to better gas mixing and a more proximal diffusion front. S1 Figure compares the linear sensitivity of LCI to airway size for both gases (computed using the perturbative method), demonstrating that the key differences between the two gases are in the acinar generations, where the diffusion front is located.

Inter-regional heterogeneity

Figure 3 (solid lines) shows the effect of constricting airways in the right-middle (RM) lobe at three different depths. Each case simulates localised bronchoconstriction, with all airways in a given generation range (proximal, central or distal) reduced in cross-section by the same fraction, approximating the pathophysiology of asthma or CF. A marked response in all three MBW indices was evident for radius constrictions above circa 70%. The responses of LCI and S_{cond} to airway constrictions were strongly correlated, peaking at approximately 80% constriction of the radius before dropping back to baseline values (Figures 3(a) and (b)), similar to the results reported in [16, 20]. This response was dominated by the resistance of the constricted airways (see S2 Figure) which resulted in under-ventilation of the affected regions, as well as asynchrony in emptying (see S1 Video and S2 Video). This response was effectively independent of constriction depth and dropped off at larger constrictions, where these regions became essentially unventilated and thus undetectable at the mouth. This is shown in Figure 3(e) by the reduction in measured FRC volume of approximately 10% (295 ml) of the lung volume.

It is a simplification to assume that constrictions or blockages would be localised to a single lobe. However, randomly distributed constrictions applied to families of airways at each depth that feed the same fraction (10%) of the lung volume, resulted in a very similar response due to the homogeneity of the baseline case (see Figures 3(b), (d) and (f)). The response was weaker than the localised case for a more distal heterogeneous distribution of constrictions, and dropped off more gradually with very large constriction sizes (>80% radius consitriction). In this case, 10% of the airways from the most proximal generation (Strahler orders 19,15,11 for proximal, central and distal cases respectively) were selected uniformly randomly, and constrictions were applied to these and the three generations

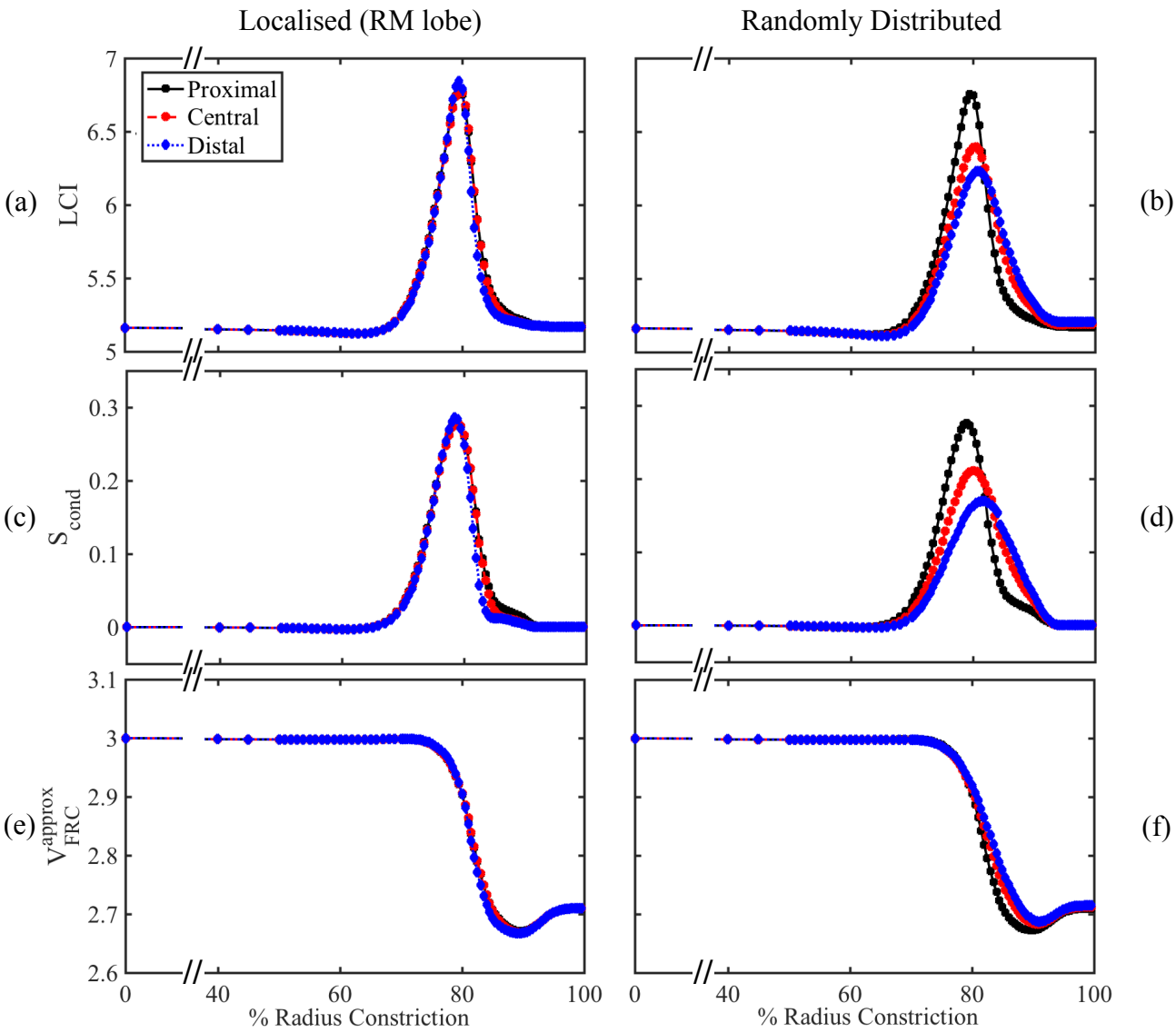

Figure 3: Relationship between constriction strength (% radius reduction) and MBW indices (a)-(b) LCI, (c)-(d) S_{cond} and (e)-(f) measured FRC volume $V_{\text{FRC}}^{\text{approx}}$ applied to airways feeding 10% of the lung acinar volume. Three different depths were tested, corresponding to Strahler order 19-16 (proximal, black squares), 15-12 (central, red circles), and 11-8 (distal, blue diamonds), where all branches constricted were taken to be directly descended from the most proximal in all cases. (a), (c) and (e) show simulations where constrictions were all localised within the right-middle lobe, whereas (b), (d), and (f) show realisations where the positions of the constrictions were uniformly randomly distributed throughout the lung. Example animations of localised and random constrictions are shown in S1 Video and S2 Video respectively.

of airways descended from them. Once constrictions had been applied to the full network, symmetric sub-trees were re-identified and replaced with mean-paths (following S1 File §1.4), as can be observed in the network structure in S2 Video. Note that these results were computed through direct simulation, and not using the perturbative approach.

To conclude, we have found that MBW indices detect a restricted range of severe airway constrictions, which our results predict to be most sensitive when airways are between 10% - 30% of their original radius.

Intra-regional heterogeneity

Figure 4 shows the predicted uncertainty in MBW indices due to airway heterogeneity. Two types of airway heterogeneity are presented: first where changes to airway lengths and areas are generated completely independently; and second where the areas and lengths are correlated with changes in the parent airways (see Figure 2 and S1 File §3 for further details). In general, the standard deviations of LCI and S_{cond} increased when airway sizes were correlated with their parent branch. Furthermore, the standard deviations showed a similar response to constrictions as the indices themselves, meaning that there was increased uncertainty due to airway heterogeneity when the indices were elevated. There was a small drop in LCI variance at $\sim 80\%$ radius constrictions, corresponding to the stationary point of the LCI curve in Figure 3(a)-(b). This means that the uncertainty showed similar behaviour to the magnitude of the gradient of the curve in Figure 3(a)-(b).

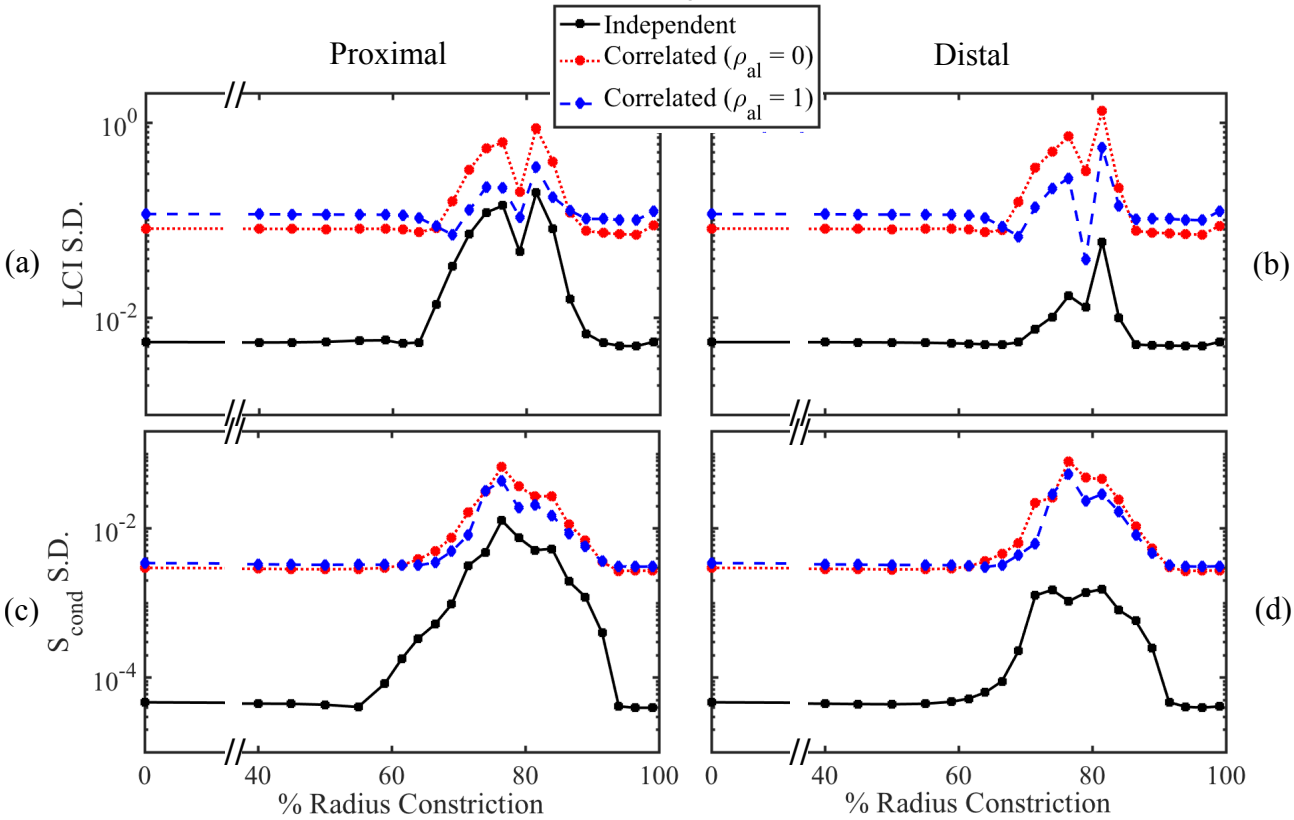

Figure 4: Standard deviation in (a)-(b) LCI and (c)-(d) S_{cond} vs. constriction strength (for constrictions confined to RM lobe). Results were computed for independent normally distributed perturbations (black squares) and structurally correlated perturbations (see S1 File §4.2) with $\rho_{al} = 0$ (diameter and length uncorrelated, red circles) and $\rho_{al} = 1$ (fixed diameter-length ratio, blue diamonds). (a) and (c) show the results for Strahler orders 19-16 (proximal) and (b) and (d) for Strahler orders 11-8 (distal, dotted line, diamonds). Constrictions were applied to all airways in the RM lobe within these generation ranges as in Figure 3. In all cases $\sigma_a = 0.2$ and $\sigma_l = 0.1$. Note the logarithmic scale on the vertical axes.

Figure 4 also shows different responses depending on constriction depth. Independently distributed airway heterogeneity has less effect on standard deviation of the indices when constrictions are more distal. However, when parent-daughter airway sizes were correlated, the effect on LCI and S_{cond} standard deviations was similar regardless of constriction depth. This implies that this type of structured heterogeneity, whereby uncertainty in airway size grows with each generation, enhances the

contribution of the smaller airways to the overall uncertainty.

Figure 4 also compares the case where airways retain a fixed length-to-diameter ratio, but there is heterogeneity in overall airway size. In this case, the standard deviations of LCI and S_{cond} did not increase by as much at severe constriction strengths. Area and length increases have opposite impacts on airway resistance, and therefore we observed opposite effects LCI and S_{cond} at severe constrictions (see S2 Figure). Thus correlated area and length changes ($\rho_{al} = 1$) did not increase the uncertainty as much as uncorrelated ($\rho_{al} = 0$) changes when severe constrictions were present.

Finally, the perturbative simulations also showed that sensitivity of the MBW indices to changes in lung elastance was increased at large constriction strength (see S3 Figure). Also, even though the constrictions were localised to the RM lobe, this increased sensitivity was observed for changes in elastance in all of the lobes.

To conclude, when the MBW indices are elevated due to severe airway constrictions, they were more sensitive to heterogeneity in both airway size and other mechanical properties such as elastance. This indicates that values measured experimentally are likely to be more variable in the presence of severe bronchoconstriction or mucus plugging.

Global Heterogeneity: Fractional Ventilation Distribution

Figure 5 shows the distribution of acinar fractional ventilation (FV) values at different constriction strengths, and for different distributions of airway heterogeneity. The dotted vertical lines in Figure 5(b)-(d) show the FV values for each region in the baseline model (no linear perturbations), while the continuous distributions show the predicted FV values by the perturbative model. As the fractional ventilation in the RM lobe decreased (and LCI increased) the distribution of FV in this lobe also broadened (Figures 5(b) and (c)), before it narrowed again at very large constrictions (Figure 5(d)). This shows that the local FV was most sensitive to airway heterogeneity in the same constriction strength range as the MBW indices. When there was fixed airway length-to-diameter ratio) the FV distribution was narrower in the constricted lobe (RM), where airway resistance dominates, and broader in the other regions, where airway dead-space volume is the dominant factor. The results clearly demonstrate a link between the width of the FV distribution and the resulting model uncertainty in MBW indices due to airway heterogeneity.

A key finding is that the unconstricted mean-paths were relatively unaffected, and remained fairly insensitive to airway heterogeneity in those paths. Nonetheless, there is a small drop in FV in the right-lower lobe, which can be explained by a pendelluft effect where gas from the right-middle lobe is re-inspired into the right-lower lobe due to the asynchronous nature of the ventilation (see S1 Video).

In summary, the FV distributions show that severe airway constrictions result in a much broader distribution of gas turnover in the affected lung region (assuming some randomness in airway geometry). Aside from the noted pendelluft affects, the distribution of FV due to airway randomness remained largely unchanged, highlighting the parallel nature of the airway network structure.

Discussion

In this paper we have introduced a perturbative approach that accounts for the uncertainty in predictions due to random variation in the lung's geometrical and mechanical properties. Our results showed that S_{cond} and LCI responded in a highly correlated manner to bronchoconstriction, whether this was localised to a single lobe or distributed across the lung (Figure 3). The response was notably non-

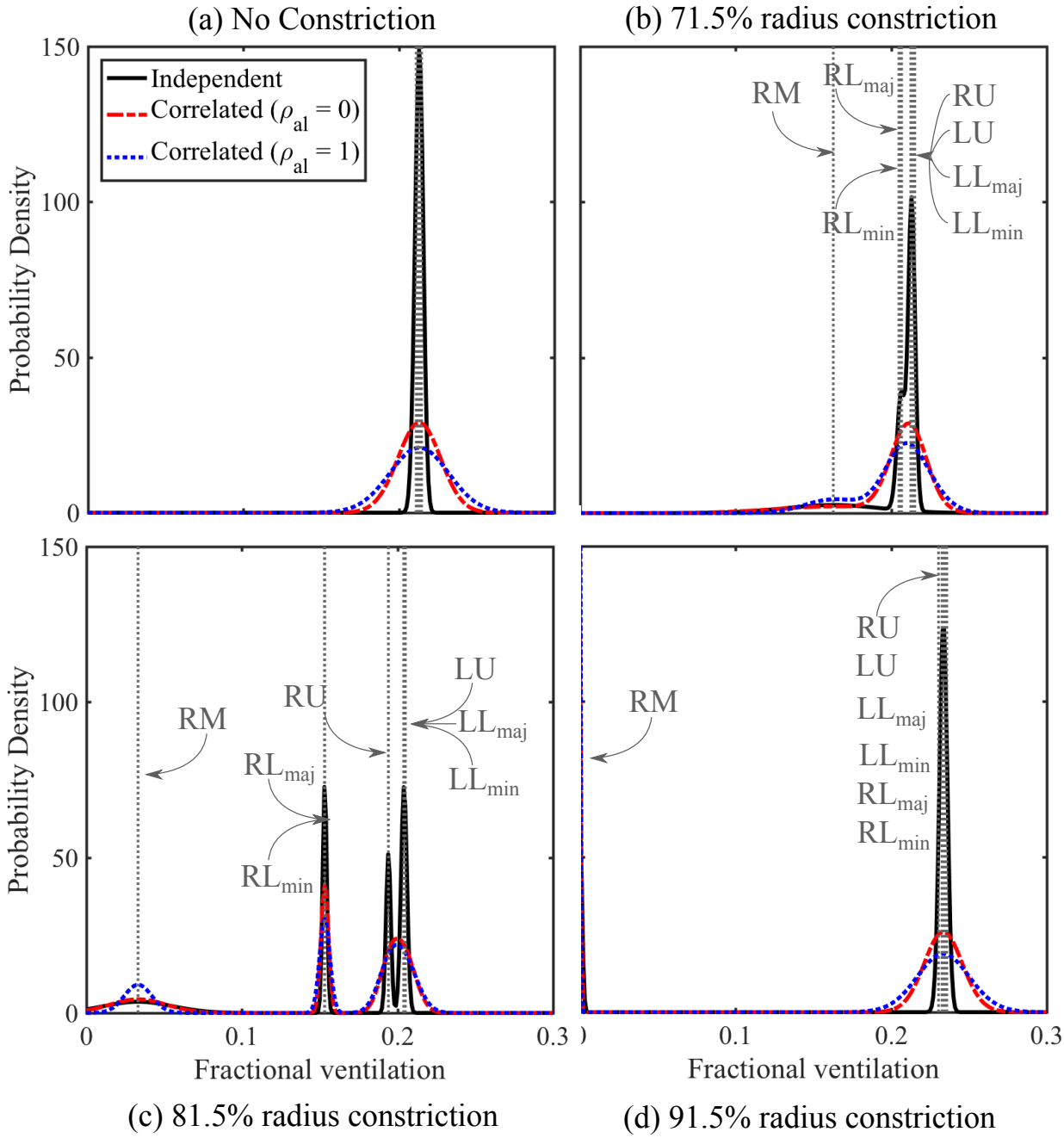

Figure 5: Whole lung fractional ventilation distributions for (a) 0% (b) 71.5% (c) 81.5%, and (d) 91.5% constrictions to the radius of the airways in the central airways of the RM lobe (central, Strahler orders 15-12). Results for independent random perturbations (solid black lines) and structurally correlated random perturbations with $\rho_{al} = 0$ (dashed red lines) and $\rho_{al} = 1$ (fixed diameter-length ratio, dotted blue lines). For visibility, $\sigma_a = 0.5$ and $\sigma_l = 0.25$ was used for the independent case, whereas $\sigma_a = 0.1$ and $\sigma_l = 0.05$ was used for the correlated case. The vertical dotted lines indicate the mean FV values in each lobar region. In (b), (c) and (d) the regions are labelled as in Figure 1.

linear, showing a high sensitivity to large-magnitude constrictions ($\sim$ 80% reduction in radius) before returning to baseline values at even larger constrictions. The sharp response is due to the inverse-fourth-power dependence of airway resistance (approximated here by Poiseuille flow) to changes in airway radius. This suggests a mechanism to explain the success of MBW indices to differentiating obstructive lung conditions such as asthma and CF, where airway inflammation and blockage is a typical feature, from healthy volunteers where such narrow airways are unlikely to be present in large

numbers. We also found that LCI and S_{cond} did not respond as strongly if constrictions were randomly distributed in the distal conducting airways, because in this case the well- and under-ventilated lung units branch from one another more distally (where advection is less dominant over diffusion) than the case where constrictions were localised.

This weak response to small airway geometry deviations motivated the use of perturbation theory to account for heterogeneity in the underlying airway structure. Using this, we found that the uncertainty in predictions due to weak heterogeneity in the structure was greatly amplified when LCI and S_{cond} were elevated due to constrictions (where we considered constrictions confined to a single lobe, see Figure 4). When the perturbations were independently distributed, the variance was greater if there were few proximal constrictions (two in this case) rather than numerous distal constrictions (2^9). This is because the indices are most sensitive to geometrical changes in the perturbed airways, which are more likely to average out due to the large number of constrictions in the latter case. On the other hand, fluctuations from the mean are much more likely to occur when there is a small number of constrictions. This uncertainty is amplified further by including structural correlations that account for the inherited nature of airway sizes (e.g. larger-than-average airways on average branch into larger-than-average airways). We found that the smaller airways appeared to contribute equally to the variance in indices in this case, because more proximal fluctuations from the mean were propagated down the airway tree.

More broadly, these results suggest that elevated MBW indices induced by airway constrictions are more variable in general, which is observed experimentally through the increased variance in LCI measured in CF and asthma patients [46], as well as an increased sensitivity of LCI to posture which affects the distribution of ventilation due to gravity [47, 48]. This latter affect can be understood by perturbing acinar elastance, which affects their rate of ventilation. S3 Figure confirmed that the magnitude of the sensitivity of the MBW indices to elastance perturbations was much larger when airways were pathologically constricted (even when the perturbations were in different lung regions to the constrictions). The former effect is more complex, as inter-subject variability is likely to be larger due to variations in disease progression and expression, which would be expected to dominate over the effects of heterogeneity in airway sizes. Additionally, in the artificial case considered here, the constriction strengths are assumed uniform and hence extra uncertainty would be introduced by including heterogeneity in constriction strength too.

Finally, we used the perturbative approach to compute probability distributions of acinar fractional ventilation values (Figure 5). The FV distributions predicted are generally narrower than measured experimentally [36]. This is in part due to the simplified nature of the mean-path model and the assumption of weak heterogeneity. Furthermore, acini sizes are also variable which directly affects their FV values, while gravitational effects also play a role [17]. However, the response we observe is indicative of the effects of heterogeneity in airway structure alone, and demonstrate the relationship between variation in structure and the distribution of FV within a lung. We saw that, generally, the FV distribution was much broader in the lung region affected by the constrictions, which is consistent with the increased variance in MBW indices predicted (Figure 4). These calculations also showed that the unconstricted regions are relatively unaffected by the presence of the blockage, due to the parallel nature of the lung structure.

The underlying model is simple, considering only seven distinct lung regions and assuming that the airway and acinar structures are symmetrical in each. However, the model is sufficient to predict some generic relationships between lung structure and the MBW indices, in particular LCI and S_{cond}.

The LCI values predicted by the model are low compared to those measured experimentally [46], but similar to those simulated in more detailed airway tree models [39, 20]. The phase-III slopes are practically zero in the absence of constrictions, whereas in a healthy lung airway asymmetry and acinar duct asymmetry both contribute to positive slopes [39]. These differences can in part be attributed to the idealised nature of this model, which assumes complete symmetry in the acinar structure. This means that mixing efficiency in the alveolar zone is better than is likely in reality, and LCI is therefore lower.

The perturbative method addresses this effect of intra-regional airway asymmetry, which is not present in the baseline model, but is valid only for small deviations of properties from the mean. As this method measures the linearised response of the model variables to changes in structure or mechanics, it misses non-linear behaviour, which can become dominant at increasing perturbation magnitude. Additionally, the number of trees one has to simulate to compute all of the linear sensitivities increases with the number of mean-paths in the baseline model. Thus there is a balance to be struck between the resolution of the baseline model (i.e. how many lung regions the mean-path model is split into) being sufficient to simulate realistic ventilation heterogeneity and computational efficiency. Nonetheless, the perturbative approach gives a unique insight into the relation between structural changes and lung function.

Other assumptions made in the model are likely to affect predicted MBW outcomes. Most significantly, we have neglected the effects of gravity/posture on inter-regional variation, as well as mechanical coupling of the lung units, which are both predicted to affect fractional ventilation and MBW indices in simulations [40, 17, 41, 42] and experiments [43, 44, 48]. The lack of mechanical coupling means that the predicted asynchrony between lung regions may be exaggerated compared to reality, which could indicate why the range of predicted S_{cond} values is notably wider than the increase measured between healthy volunteers and CF patients [50]. Furthermore, air flow has been modelled by the Poiseuille relation in all airways, meaning that the effects of inertia [38] and turbulent flow are neglected. Finally, we have not include the effects of gas exchange on inert gas transport, as it is thought to be negligible (except in the case where nitrogen is used as the MBW tracer gas [49]). The limitations imposed by these assumptions are discussed in more detail in S1 File.

Conclusion

The strength of the perturbative approach introduced in this paper is two-fold. First, it reduces simulation complexity, as the maximum number of terminal airways to be simulated scales linearly with generation rather than exponentially. Second, once the linear sensitivities are calculated for a given simulation, they can be combined in numerous ways to investigate the effects of different patterns of heterogeneity. This avoids the need to randomly generate many realisations of a higher-resolution model, as would be required if using Monte-Carlo sampling.

In future, this approach will be further developed to quantify uncertainty in more realistic lung models that are directly informed by imaging data. The principles outlined here will enable a systematic approach that quantifies uncertainty due to both the intrinsic complexity of lung structure and the additional effects of obstructive lung disease or gravity.

Acknowledgments

The authors would like to thank Dr Tobias Galla for his contributions to the early stages of this project. Furthermore, we acknowledge fruitful discussions with Prof Jim Wild and Dr Guilhem Collier.

CW was funded by the UK Medical Research Council (MRC) grant number MR/R024944/1. CW and OE acknowledge the UK Engineering and Physical Sciences Research Council (EPSRC) for funding through grant reference EP/K037145/1. AH was funded by a UK National Institute for Health Research (NIHR) Clinician Scientist (CS012-13). This report presents independent research funded by the NIHR. The views expressed are those of the authors and not necessarily those of the UK National Health Service, the NIHR or the UK Department of Health.

Supporting information

S1 Table List of parameters and values used in simulations.

Parameter	**Description**	**Values used**
V_{FRC}	Total lung and mouth cavity volume at rest.	3 L
V_D	Total volume of conducting airways.	0.12 L
V_{mouth}	Total volume of mouth cavity.	0.05 L
V_T	Tidal volume.	1L
τ	Breath time (inhalation or exhalation).	2.5 s
$V_{\text{duct}}/V_{\text{acin}}$	Proportion of acinar gas volume in ducts.	0.2 [3]
λ_{cond}	Airway length scaling in mean-path conducting branches.	0.794 [8]
λ_{acin}	Duct length scaling in acinar branches.	0.93 [3]
LD_{cond}	Ratio of length to diameter in mean-path conducting branches.	3 [9, 51]
LD_{acin}	Ratio of length to diameter in acinar branches.	2.3 [3]
$N^{\text{acin}} + 1$	Number of acinar airway generations.	9 [3]
Φ_j	Density of alveolar sacs. in acinar generations. $j = N_z^{\text{cond}} \dots N^{\text{tot}}$.	0 if $j < N_z^{\text{cond}}$ 0.2 if $j = N_z^{\text{cond}}$ 0.4 if $j = N_z^{\text{cond}} + 1$ [3] 0.7 if $j = N_z^{\text{cond}} + 2$ 1 if $j > N_z^{\text{cond}} + 2$
ϕ	Phenomenological parameter, see equation (10) in S1 File.	0.5 [15]
K	Elasticity of the whole lung.	5 cm H_2O L^{-1} [52, 53]
R_{acin}	Cumulative resistance of acini.	0.2 cm H_2O s L^{-1} [54, 52]
R_{UA}	Resistance of the upper airway.	0.6 cm H_2O s L^{-1} [54, 52]
μ	Air viscosity at 37°C.	1.93×10^{-7}cm H_2O s
$\{d, l\}$ Diameters and lengths of proximal bronchi (cm)	Trachea Right Main Bronchus Left Main Bronchus Right Intermediate Bronchus Right Lower Lobar Bronchus Left Lower Lobar Bronchus	{1.6, 10} {1.11, 2.2} {1.2, 5} [9] {0.89, 2.6} {0.64, 0.8} {0.8, 1.1}

S1 Figure Linear fractional change in LCI due to a single perturbation in area ((a) and (c)) and length ((b) and (d)) scaled by number of branches in that generation N_b. The airway generation is plotted in terms of its Strahler order (*i.e.* its generation counting up from zero at the bottom of the tree). The vertical dashed line indicate the terminal bronchiole separating the acinar (Strahler orders 0-8) and conducting (>9) generations. (a)-(b) Healthy lung model using SF_6 (molecular diffusivity 0.105cm^2 s^{-1}). (c)-(d) Healthy lung model using N_2 (molecular diffusivity 0.225cm^2 s^{-1}). Coloured symbols distinguish perturbations in the seven lobar regions. The LCI sensitivities in the conducting region (right of the vertical dashed line) are approximately identical for area and length perturbations in both cases, as this is a response to the increase in dead-space volume. For SF_6 the sensitivities in the acinar region (left of the vertical dashed line) are inverted for length and area perturbations, most notably around the diffusion front (approximately Strahler order 4). Thus LCI is sensitive to geometry changes that affect diffusion in the acinus when using the less diffusive SF_6, but not N_2.

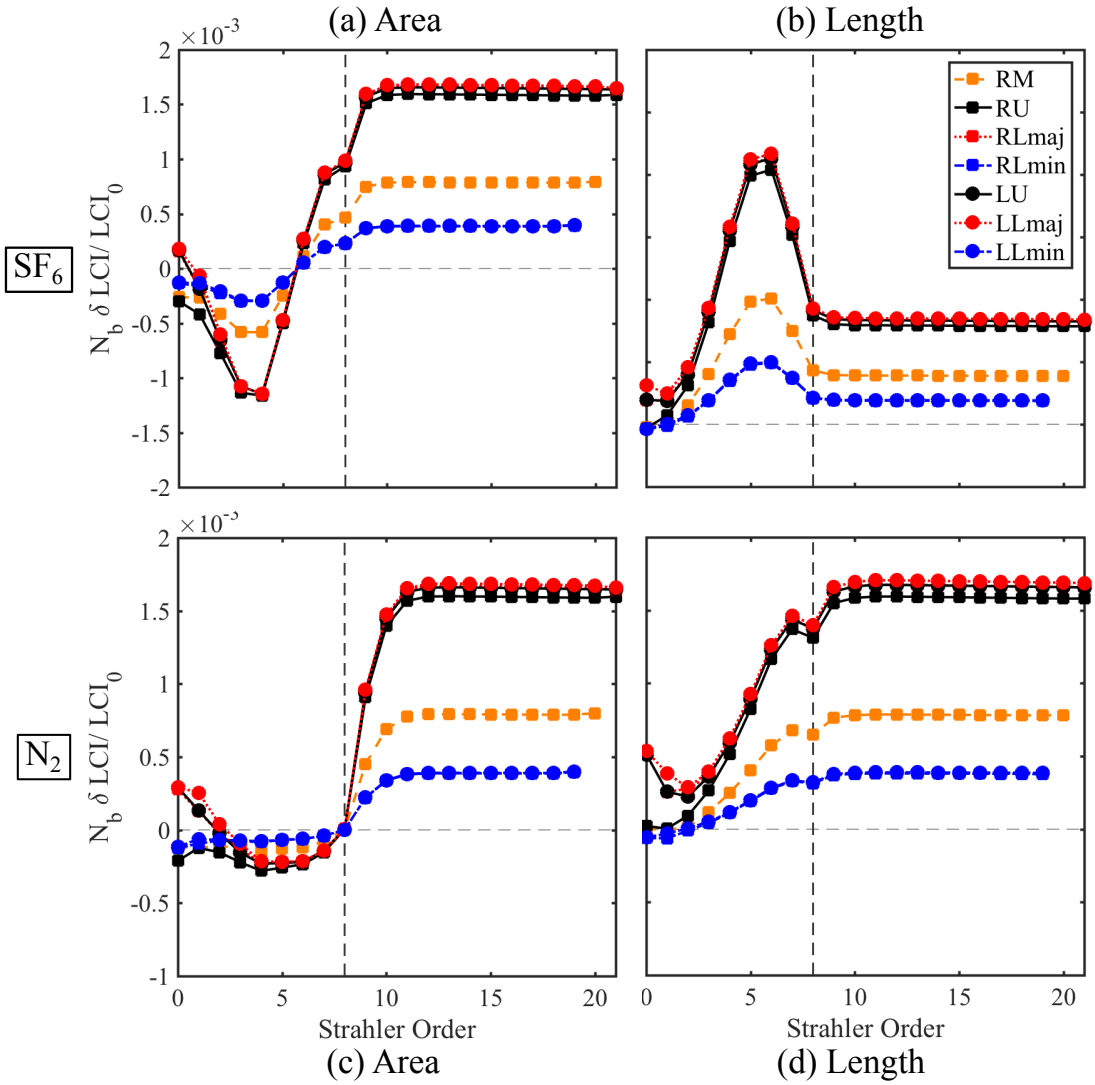

S2 Figure Linear sensitivities to geometry perturbations in a model realisation with (a)-(b) 74% and (c)-(d) 81.5% constrictions in radius to the RM lobe. Scaled sensitivities (as in S1 Figure) w.r.t. area (filled markers) and length (open markers) of the airways are shown for the RM lobe only for fractional LCI change and absolute change in S_{cond}. Results were plotted for different depths of constriction: proximal (Strahler orders 16-19, black squares), central (Strahler orders 12-15, red circles) and distal (Strahler orders 8-11, blue diamonds). The sensitivities are scaled by the number of airways in the corresponding Strahler order of the RM lobe. The scaled sensitivities are much larger in the constricted airways, as the response is most sensitive to their resistance (note the difference in scale to S1 Figure). Since airway resistance scales as length/area^2, the area sensitivities are approximately a factor -2 of the length sensitivities. The sign of the sensitivities changes between the two constriction strengths because they lie either side of the maximum values of LCI and S_{cond} in Figure 3(a) and (b).

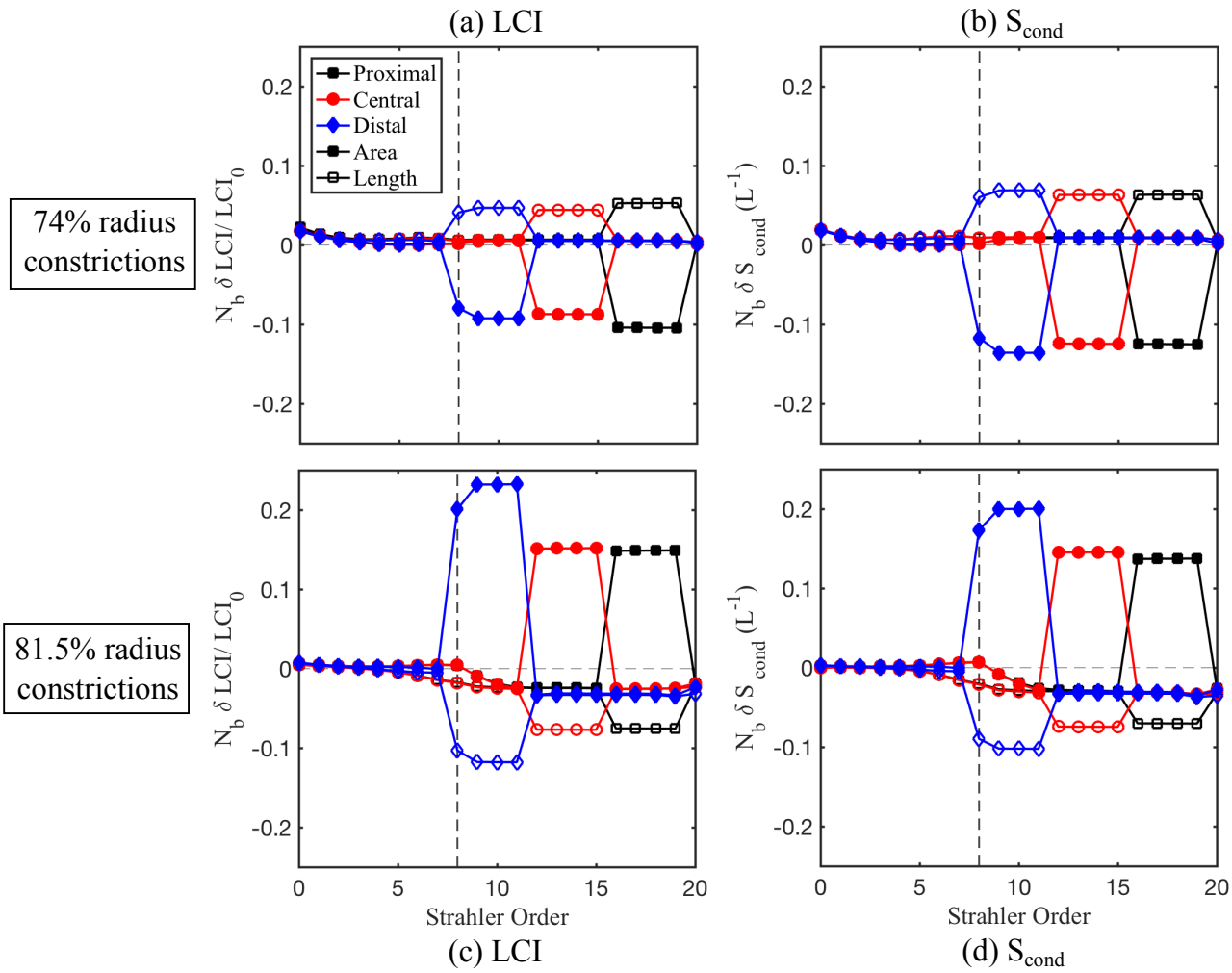

S3 Figure Sensitivity of LCI to changes in elastance of an acinus in each mean-path vs. constriction strength of the central airways in the RM lobe. Linear sensitivities were scaled by the number of acini N_b in the perturbed lobar region. The sensitivity increased in size by an order of magnitude upon increasing constriction size. As constriction strength was increased, an increase in elasticity of the RM lobe decreased flow to that lobe, further increasing ventilation heterogeneity and LCI. Meanwhile increases to elasticity in other lobes increased the flow to RM and decreased LCI. Once the constriction strength is $> 75\%$ the effect reversed because increases in the flow to the RM lobe released trapped gas that would have otherwise been undetectable by MBW.

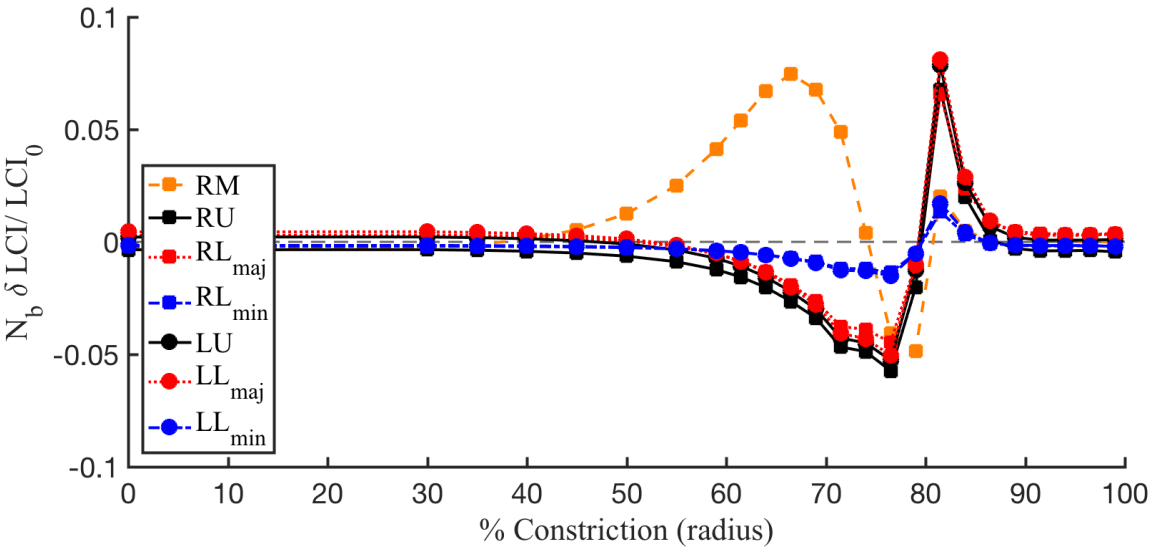

S1 Video Inert gas concentration on lung network for various constriction strengths to the central airways of the RM lobe (% reduction in radius as shown). Vertical direction is the distance from the mouth, while horizontal distances have no physical meaning and are set for visibility. Time scale 1:4 (each second of video corresponds to 4 seconds of washout).

S2 Video Inert gas concentration on lung network at varying constriction strengths in the central airways distributed throughout the lung (% reduction in radius as shown). Vertical direction is the distance from the mouth, while horizontal distances have no physical meaning and are set for visibility.. Time scale 1:4 (each second of video corresponds to 4 seconds of washout).

S1 File Supplementary text containing further details of the methodology.

References

[1] Haefeli-Bleuer B, Weibel ER. Morphometry of the human pulmonary acinus. Anat. Rec. 1988;220(4):401–414. doi:10.1002/ar.1092200410.

[2] Murray CD. The Physiological Principle of Minimum Work: I. The Vascular System and the Cost of Blood Volume. PNAS. 1926;12(3):207–14. pmid:16576980.

[3] Hsia CCW, Hyde DM, Weibel ER. Lung Structure and the Intrinsic Challenges of Gas Exchange. In: Compr. Physiol.. vol. 6. Hoboken, NJ, USA: John Wiley & Sons, Inc.; 2016. p. 827–895. doi:10.1002/cphy.c150028.

[4] Marshall H, Horsley A, Taylor CJ, Smith L, Hughes D, Horn FC, et al. Detection of early subclinical lung disease in children with cystic fibrosis by lung ventilation imaging with hyperpolarized gas MRI. Thorax. 2017;72(8):6–9. doi:10.1136/thoraxjnl-2016-208948.

[5] Teague WG, Tustison NJ, Altes TA. Ventilation heterogeneity in asthma. J Asthma. 2014;51(7):677–684. doi:10.3109/02770903.2014.914535.

[6] Horsley A, Wild JM. Ventilation heterogeneity and the benefits and challenges of multiple breath washout testing in patients with cystic fibrosis. Paediatr Respir Rev. 2015;16:15–18. doi:10.1016/j.prrv.2015.07.010.

[7] Robinson PD, Latzin P, Verbanck S, Hall GL, Horsley A, Gappa M, et al. Consensus statement for inert gas washout measurement using multiple- and single- breath tests. Eur Respir J. 2013;41(3):507–522. doi:10.1183/09031936.00069712.

[8] Weibel ER. Morphometry of the Human Lung. 1st ed. Springer-Verlag Berlin Heidelberg; 1963.

[9] Horsfield K, Dart G, Olson DE, Filley GF, Cumming G. Models of the human bronchial tree. J Appl Physiol. 1971;31(2):207–217. doi:10.1152/jappl.1971.31.2.207

[10] Yu CP. On equation of gas transport in the lung. Respir Physiol. 1975;23(2):257–266. doi:10.1016/0034-5687(75)90064-X.

[11] Wagner PD. Information content of the multibreath nitrogen washout. J Appl Physiol. 1979;46(3):579–87. doi:10.1152/jappl.1979.46.3.579

[12] Paiva M, Engel LA. Influence of bronchial asymmetry on cardiogenic gas mixing in the lung. Respir Physiol. 1982;49(3):325–338. doi:10.1016/0034-5687(82)90120-7.

[13] Neufeld GR, Schwardt JD, Gobran SR, Baumgardner JE, Schreiner MS, Aukburg SJ, et al. Modelling steady state pulmonary elimination of He, SF6 and CO2: Effect of morphometry. Respir Physiol. 1992;88(3):257–275. doi:10.1016/0034-5687(92)90001-D.

[14] Dutrieue B, Vanholsbeeck F, Verbanck S, Paiva M. A human acinar structure for simulation of realistic alveolar plateau slopes. J Appl Physiol. 2000;89(5):1859–67. doi:10.1152/jappl.2000.89.5.1859

[15] Henry FS, Llapur CJ, Tsuda A, Tepper RS. Numerical Modelling and Analysis of Peripheral Airway Asymmetry and Ventilation in the Human Adult Lung. J Biomech Eng. 2012;134(6):061001. doi:10.1115/1.4006809.

[16] Mitchell JH, Hoffman EA, Tawhai MH. Relating indices of inert gas washout to localised bronchoconstriction. Respir Physiol Neurobiol. 2012;183(3):224–233. doi:10.1016/j.resp.2012.06.031.

[17] Swan AJ, Clark AR, Tawhai MH. A computational model of the topographic distribution of ventilation in healthy human lungs. J Theor Biol. 2012;300:222–231. doi:10.1016/j.jtbi.2012.01.042.

[18] Kim M, Bordas R, Vos W, Hartley RA, Brightling CE, Kay D, et al. Dynamic flow characteristics in normal and asthmatic lungs. Int J Numer Meth Biomed Eng. 2015;31(12):e02730. doi:10.1002/cnm.2730.

[19] Roth CJ, Ismail M, Yoshihara L, Wall WA. A comprehensive computational human lung model incorporating inter-acinar dependencies: Application to spontaneous breathing and mechanical ventilation. Int J Numer Meth Biomed Eng. 2017;33(1):e02787. doi:10.1002/cnm.2787.

[20] Foy BH, Kay D, Bordas R. Modelling responses of the inert-gas washout and MRI to bronchoconstriction. Respir Physiol Neurobiol. 2017;235:8–17. doi:10.1016/j.resp.2016.09.009.

[21] Maury B. The Respiratory System in Equations. Milano: Springer Milan; 2013. Available from: `http://link.springer.com/10.1007/978-88-470-5214-7`.

[22] Guennebaud G, Jacob B, Others. Eigen; 2010. Available from: `http://eigen.tuxfamily.org`.

[23] Verbanck S, Paiva M. Model simulations of gas mixing and ventilation distribution in the human lung. J Appl Physiol. 1990;69(6):2269–79. doi:10.1152/jappl.1990.69.6.2269

[24] Tippe A, Tsuda A. Recirculating flow in an expanding alveolar model: Experimental evidence of flow-induced mixing of aerosols in the pulmonary acinus. J Aerosol Sci. 2000;31(8):979–986. doi:10.1016/S0021-8502(99)00572-8.

[25] Weibel ER, Sapoval B, Filoche M. Design of peripheral airways for efficient gas exchange. Respir Physiol Neurobiol. 2005;148(1-2 SPEC. ISS.):3–21. doi:10.1016/j.resp.2005.03.005.

[26] Tsuda A, Henry FS, Butler JP. Gas and aerosol mixing in the acinus. Respir Physiol Neurobiol. 2008;163(1-3):139–149. doi:10.1016/j.resp.2008.02.010.

[27] Sznitman J. Convective gas transport in the pulmonary acinus: Comparing roles of convective and diffusive lengths. J Biomech. 2009;42(6):789–792. doi:10.1016/j.jbiomech.2008.12.022.

[28] Paiva M. Gas transport in the human lung. J Appl Physiol. 1973;35(3):401–10. doi:10.1152/jappl.1973.35.3.401

[29] Scherer PW, Shendalman LH, Greene NM, Bouhuys A. Measurement of axial diffusivities in a model of the bronchial airways. J Appl Physiol. 1975;38(4):719–23. doi:10.1152/jappl.1975.38.4.719

[30] Becklake MR. A new index of the intrapulmonary mixture of inspired air. Thorax. 1952;7(1):111–6. doi:10.1136/thx.7.1.111.

[31] Horsley A. Lung clearance index in the assessment of airways disease. Respir Med. 2009;103(6):793–799. doi:10.1016/j.rmed.2009.01.025.

[32] Engel LA. Gas mixing within the acinus of the lung. J Appl Physiol. 1983;54(3):609–618. doi:10.1152/jappl.1983.54.3.609.

[33] Crawford A, Makowska M. Convection-and diffusion-dependent ventilation maldistribution in normal subjects. J Appl Physiol. 1985;59(3):838–846. doi:10.1152/jappl.1985.59.3.838

[34] Verbanck S, Schuermans D, Van Muylem A, Paiva M, Noppen M, Vincken W. Ventilation distribution during histamine provocation. J Appl Physiol. 1997;83(6):1907–16. doi:10.1152/jappl.1997.83.6.1907

[35] Deninger AJ, Månsson S, Petersson JS, Pettersson G, Magnusson P, Svensson J, et al. Quantitative measurement of regional lung ventilation using 3He MRI. Magn Reson Med. 2002;48(2):223–232. doi:10.1002/mrm.10206.

[36] Horn FC, Deppe MH, Marshall H, Parra-Robles J, Wild JM. Quantification of regional fractional ventilation in human subjects by measurement of hyperpolarized 3He washout with 2D and 3D MRI. J Appl Physiol. 2014;116(2):129–139. doi:10.1152/japplphysiol.00378.2013.

[37] Koblinger L, Hofmann W. Aerosol deposition calculations with a stochastic lung model. Acta Phys Hungarica. 1986;59(1):31–34. doi:10.1007/BF03055180.

[38] Pedley TJ, Schroter RC, Sudlow MF. The prediction of pressure drop and variation of resistance within the human bronchial airways. Respir Physiol. 1970;9(3):387–405. doi:10.1016/0034-5687(70)90094-0.

[39] Tawhai MH, Hunter PJ. Multibreath washout analysis: modelling the influence of conducting airway asymmetry. Respir Physiol. 2001;127(2-3):249–258. doi:10.1016/S0034-5687(01)00239-0.

[40] Tawhai MH, Nash MP, Lin CL, Hoffman EA. Supine and prone differences in regional lung density and pleural pressure gradients in the human lung with constant shape. J Appl Physiol. 2009;107(3):912–920. doi:10.1152/japplphysiol.00324.2009.

[41] Yoshihara L, Roth CJ, Wall WA. Fluid-structure interaction including volumetric coupling with homogenised subdomains for modeling respiratory mechanics. Int J Numer Meth Biomed Eng. 2017;33(4):1–20. doi:10.1002/cnm.2812.

[42] Pozin N, Montesantos S, Katz I, Pichelin M, Vignon-Clementel I, Grandmont C. A tree-parenchyma coupled model for lung ventilation simulation. Int J Numer Meth Biomed Eng. 2017; p. e2873. doi:10.1002/cnm.2873.

[43] Gustafsson PM, Eiken O, Grönkvist M. Effects of hypergravity and anti-G suit pressure on intraregional ventilation distribution during VC breaths. J Appl Physiol. 2001;91(2):637–644. doi:10.1152/jappl.2001.91.2.637

[44] Grönkvist M, Bergsten E, Gustafsson PM. Effects of body posture and tidal volume on inter- and intraregional ventilation distribution in healthy men. J Appl Physiol. 2002;92(2):634–42. doi:10.1152/japplphysiol.00161.2001.

[45] Whitfield CA. PULMsim v1.1; 2018. doi:10.5281/zenodo.1251974.

[46] Horsley aR, Gustafsson PM, Macleod Ka, Saunders C, Greening aP, Porteous DJ, et al. Lung clearance index is a sensitive, repeatable and practical measure of airways disease in adults with cystic fibrosis. Thorax. 2007;63(2):135–140. doi:10.1136/thx.2007.082628.

[47] Smith L, Marshall H, Aldag I, Horn F, Collier G, Hughes D, et al. Longitudinal Assessment of Children with Mild CF Using Hyperpolarised Gas Lung MRI and LCI. Am J Respir Crit Care Med. 2017; p. rccm.201705–0894LE. doi:10.1164/rccm.201705-0894LE.

[48] Ramsey KA, McGirr C, Stick SM, Hall GL, Simpson SJ. Effect of posture on lung ventilation distribution and associations with structure in children with cystic fibrosis. J Cyst Fibros. 2017;16(6):713–718. doi:10.1016/j.jcf.2017.01.013.

[49] Scherer PW, Neff JD, Baumgardner JE, Neufeld GR. The importance of a source term in modeling multibreath inert gas washout. Respir Physiol. 1996;103(1):99–103. doi:10.1016/0034-5687(95)00080-1.

[50] Horsley AR, Macleod KA, Robson AG, Lenney J, Bell NJ, Cunningham S, et al. Effects of cystic fibrosis lung disease on gas mixing indices derived from alveolar slope analysis. Respir Physiol Neurobiol. 2008;162(3):197–203. doi:10.1016/j.resp.2008.06.014.

[51] Florens M, Sapoval B, Filoche M. Optimal branching asymmetry of hydrodynamic pulsatile trees. Phys Rev Lett. 2011;106(17):1–4. doi:10.1103/PhysRevLett.106.178104.

[52] Cotes JE, Chinn DJ, Miller MR. Lung Function. Oxford, UK: Blackwell Publishing Ltd.; 2006. Available from: `http://doi.wiley.com/10.1002/9781444312829`.

[53] Galetke W, Feier C, Muth T, Ruehle KH, Borsch-Galetke E, Randerath W. Reference values for dynamic and static pulmonary compliance in men. Respir Med. 2007;101(8):1783–1789. doi:10.1016/j.rmed.2007.02.015.

[54] Ritz T, Dahme B, Dubois AB, Folgering H, Fritz GK, Harver A, et al. Guidelines for mechanical lung function measurements in psychophysiology. Psychophysiology. 2002;39(5):546–567. doi:10.1017/S0048577202010715.